

**Unprecedented interweaving of single-helical and unequal
double-helical chains into chiral metal-organic open frameworks
with multi-walled tubular structures**

**Su-Na Wang^[a], Hang Xing^[a], Yi-Zhi Li^[a], Junfeng Bai*^[a], Manfred Scheer*^[b], Yi Pan^[a],
Xiao-Zeng You^[a]**

[a] State Key Laboratory of Coordination Chemistry, School of Chemistry and
Chemical Engineering, Nanjing University, Nanjing, 210093, P. R. China

E-mail: bjunfeng@nju.edu.cn

[b] Institut für Anorganische Chemie der Universität Regensburg, 93040 Regensburg
Germany E-mail: manfred.scheer@chemie.uni-regensburg.de

Experimental Section.

(a) The ligand H₃TTG was prepared according to the described method.
(Reference: Clark, D. R. U. S. Patent 4 402 907, **1983**.)

(b) Blue-green and orange hexagonal prism crystals of complexes **1** and **2** were obtained, respectively. The crystals were filtered, washed with distilled water, and dried in air.

Complex **1**: Yield: 45% (based on Ni(OAc)₂·6H₂O); elemental analysis (%) calcd for C₄₄H₆₆N₁₆O₂₁Ni₂ : C 41.53, H 5.23, N 17.61; found: C 41.32, H 5.26, N 17.24; IR (KBr pellet): 3406, 2927, 1671, 1617, 1588, 1558, 1398, 1310 cm⁻¹.

Complex **2**: Yield: 60% (based on CoCl₂·6H₂O); elemental analysis (%) calcd for C₄₄H₆₆N₁₆O₂₁Co₂ : C 41.51, H 5.23, N 17.60; found: C 41.67, H 5.32, N 17.38; IR (KBr pellet): 3411, 2928, 1669, 1611, 1589, 1557, 1399, 1309 cm⁻¹.

(c) Crystal data of the complexes were measured on a Bruker SMART Apex2 diffractometer at 291K using graphite-monochromated MoK_α radiation, respectively. Data reduction was performed with the Bruker SAINT package. The structures were solved with direct methods and refined with full-matrix least-squares technique using the SHELXS-97 and SHELXL-97 programs, respectively (References: Sheldrick, G. M. *SHELXS-97, Program for Crystal Structure Solution*; Göttingen University: Göttingen, Germany, **1997**; Sheldrick, G. M. *SHELXL-97, Program for Crystal Structure Refinement*; Göttingen University: Göttingen, Germany, **1997**). The coordinates of the non-hydrogen atoms were refined anisotropically, and hydrogen atoms were located in the calculated positions.

(d) Preliminary Kurtz powder second harmonic generation (SHG) measurements were carried out using the using the 1064 nm fundamental wavelength from a Nd: YAG laser.

Table S1. Selected bond lengths (\AA) and angles ($^\circ$) of complex **1** and **2**.

		Complex 1	
Ni(1)-O(1)	2.053(3)	O(1)-Ni(1)-N(7)	88.20(12)
Ni(1)-N(7)	2.103(3)	O(1)-Ni(1)-O(1W)	90.09(11)
Ni(1)-O(1W)	2.075(3)	O(1)-Ni(1)-O(1C)	177.88(17)
Ni(2)-O(3)	2.080(3)	O(1W)-Ni(1)-N(7)	86.08(12)
Ni(2)-N(8)	2.083(3)	N(7)-Ni(1)-N(7C)	92.22(18)
Ni(2)-O(2W)	2.066(3)	O(1WC)-Ni(1)-N(7C)	86.08(12)
		O(1W)-Ni(1)-N(7C)	176.20(14)
		O(3)-Ni(2)-O(2W)	88.83(12)
		O(3)-Ni(2)-O(3D)	92.10(15)
		O(3)-Ni(2)-N(8)	179.32(12)
		O(2W)-Ni(2)-N(8)	91.75(13)
		O(2W)-Ni(2)-O(3D)	88.26(12)
		O(2W)-Ni(2)-N(8D)	91.12(13)
		N(8D)-Ni(2)-N(8)	91.38(18)
		Complex 2	
Co(1)-O(1)	2.062(3)	O(1)-Co(1)-N(7)	88.05(11)
Co(1)-N(7)	2.124(3)	O(1)-Co(1)-O(1W)	89.77(10)
Co(1)-O(1W)	2.089(3)	O(1)-Co(1)-O(1C)	177.59(10)
Co(2)-O(3)	2.089(2)	O(1W)-Co(1)-N(7)	85.97(11)
Co(2)-N(8)	2.088(3)	N(7)-Co(1)-N(7C)	92.39(16)
Co(2)-O(2W)	2.068(3)	O(1WC)-Co(1)-N(7C)	85.97(11)
		O(1W)-Co(1)-N(7C)	175.82(17)
		O(3)-Co(2)-O(2W)	88.83(9)
		O(3)-Co(2)-O(3D)	92.50(14)
		O(3)-Co(2)-N(8)	179.26(11)
		O(2W)-Co(2)-O(3D)	88.97(11)
		O(2W)-Co(2)-N(8D)	91.27(11)
		O(2W)-Co(2)-N(8)	91.64(11)
		N(8D)-Co(2)-N(8)	91.62(16)

Symmetry codes: C:-y+1, -x+1, -z+13/6; D:x, x-y+1, -z+11/6.

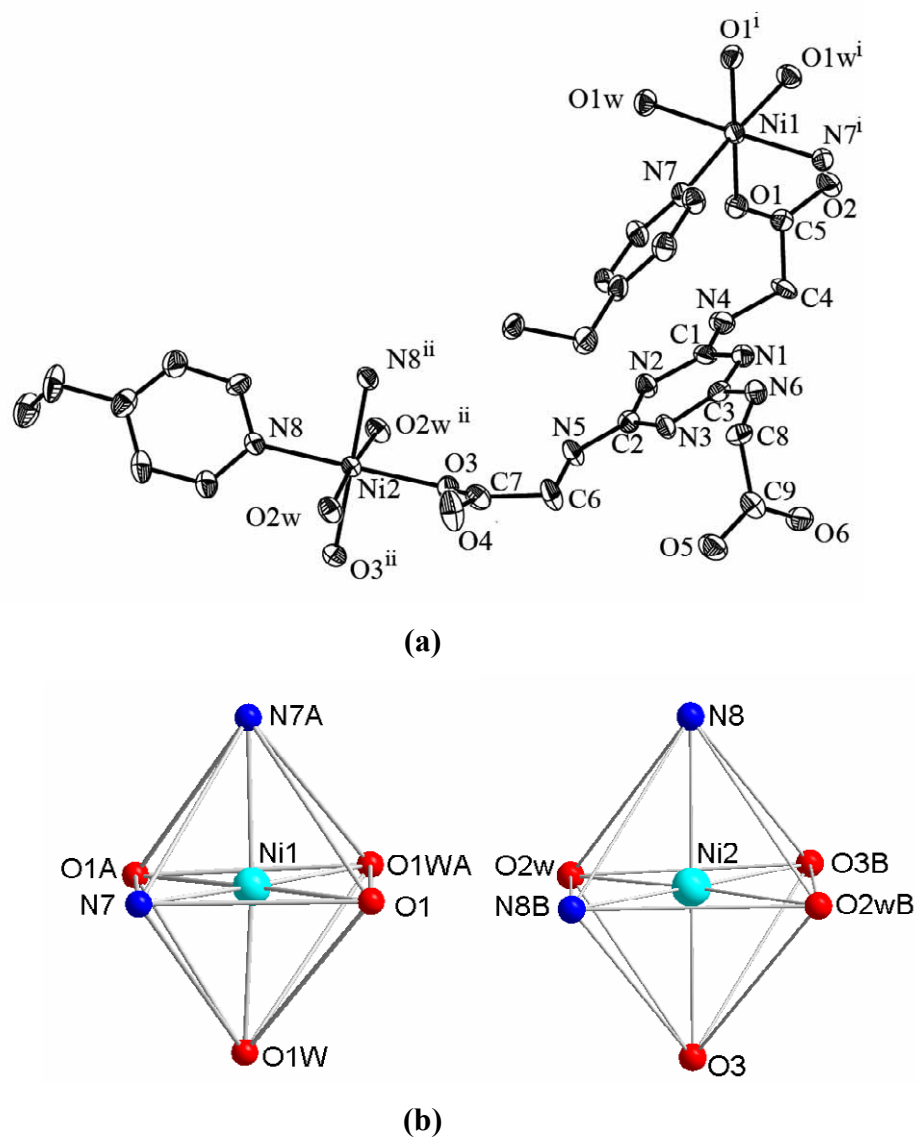
Table S2. Geometrical parameters of hydrogen bonds of the helical water chains in **1** and **2** (in Å and deg).

D-H···A	<DHA	d(D···A)
N(5)-H(5A)···O(6) ^a	160.2	2.844(5)
O(1W)-H(1WA)···O(3) ^a	158.8	2.785(4)
O(5)-H(5)···N(2) ^b	151.4	2.649(5)
O(1W)-H(1WB)···O(2) ^c	137.9	2.627(5)
O(2W)-H(2WA)···O(4)	151.2	2.632(5)
O(2W)-H(2WB)···O(6) ^d	152.7	2.661(4)
O(3W)-H(3WA)···O(4W)	120.6	2.619(8)
O(4W)-H(4WA)···O(4)	175.9	2.897(8)
O(4W)-H(4WB)···O(5W) ^e	112.2	2.805(10)
O(5W)-H(5WA)···O(2)	148.2	2.788(7)
O(5W)-H(5WB)···O(4W) ^f	114.5	2.805(10)

D-H···A	<DHA	d(D···A)
N(5)-H(5A)···O(6) ^a	161.4	2.841(4)
O(1W)-H(1WA)···O(3) ^a	159.6	2.781(4)
O(5)-H(5)···N(2) ^b	151.5	2.675(4)
O(1W)-H(1WB)···O(2) ^c	135.1	2.636(4)
O(2W)-H(2WA)···O(4)	150.9	2.648(4)
O(2W)-H(2WB)···O(6) ^d	150.4	2.683(4)
O(3W)-H(3WA)···O(4W)	122.3	2.638(5)
O(4W)-H(4WA)···O(4)	175.9	2.916(6)
O(4W)-H(4WB)···O(5W) ^e	113.2	2.781(7)
O(5W)-H(5WA)···O(2)	148.9	2.816(6)
O(5W)-H(5WB)···O(4W) ^f	111.2	2.781(7)

Symmetry codes: ^ax-y+1, -y+1, -z+1; ^bx-y, -y+1, -z+1; ^c-y+1, -x+1, -z+7/6; ^dx-y+1, x+1, z-1/6; ^ex-y, x+1, z-1/6; ^fy-1, -x+y-1, z+1/6.

Figure S1. (a) The asymmetric unit of complex **1**. Solvent water molecules and hydrogen atoms are omitted for clarity. (Symmetry codes: i, $-y + 1, -x + 1, -z + 13/6$; ii, $x, x - y + 1, -z + 11/6$.) (b) Coordination isomerism of Ni1 and Ni2 centers in complex **1**.



Both metal centers possess an octahedral geometry with the same coordination environment of $\text{Ni}\{\text{N}_2\text{O}_4\}$ moieties: two monodentate carboxylate oxygen atoms from distinct HTTG ligands, two nitrogen atoms from different bpp ligands as well as two water molecules. Arrangements of the ligands are different, however. For Ni1 center, the carboxylate oxygen atoms (O1, O1A) occupy the *trans* positions of the octahedron and the nitrogen atoms (N7, N7A) are in the *cis* ones, whilst for Ni2 center, both of the carboxylate oxygen atoms (O3, O3B) and the nitrogen atoms (N8, N8B) are situated in the *trans* positions (Symmetry codes: A, $-y + 1, -x + 1, -z + 13/6$; B, $x, x - y + 1, -z + 11/6$.)

Figure S2. Scheme representation of the combination of the metal-acid and metal-base chains into three-dimensional network viewed down the *c* axis.

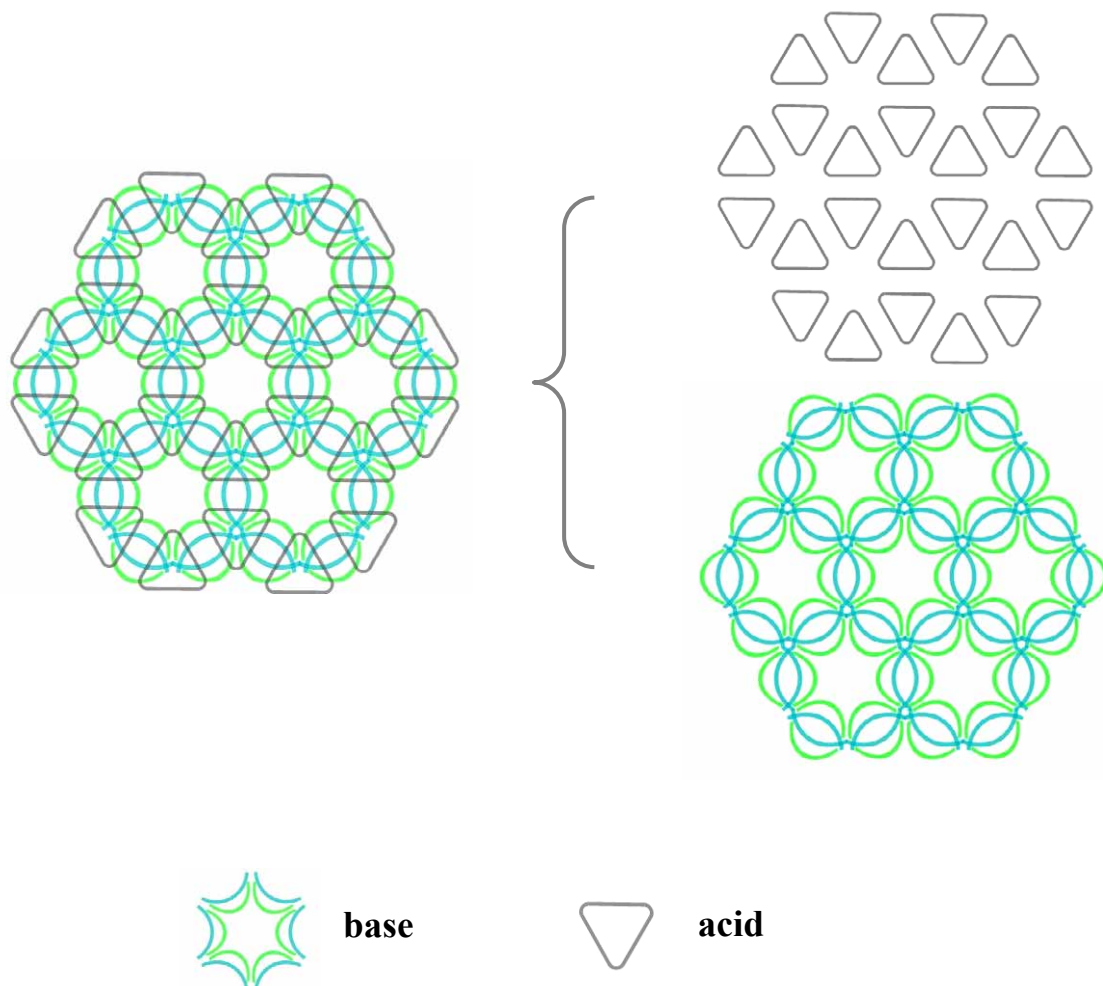
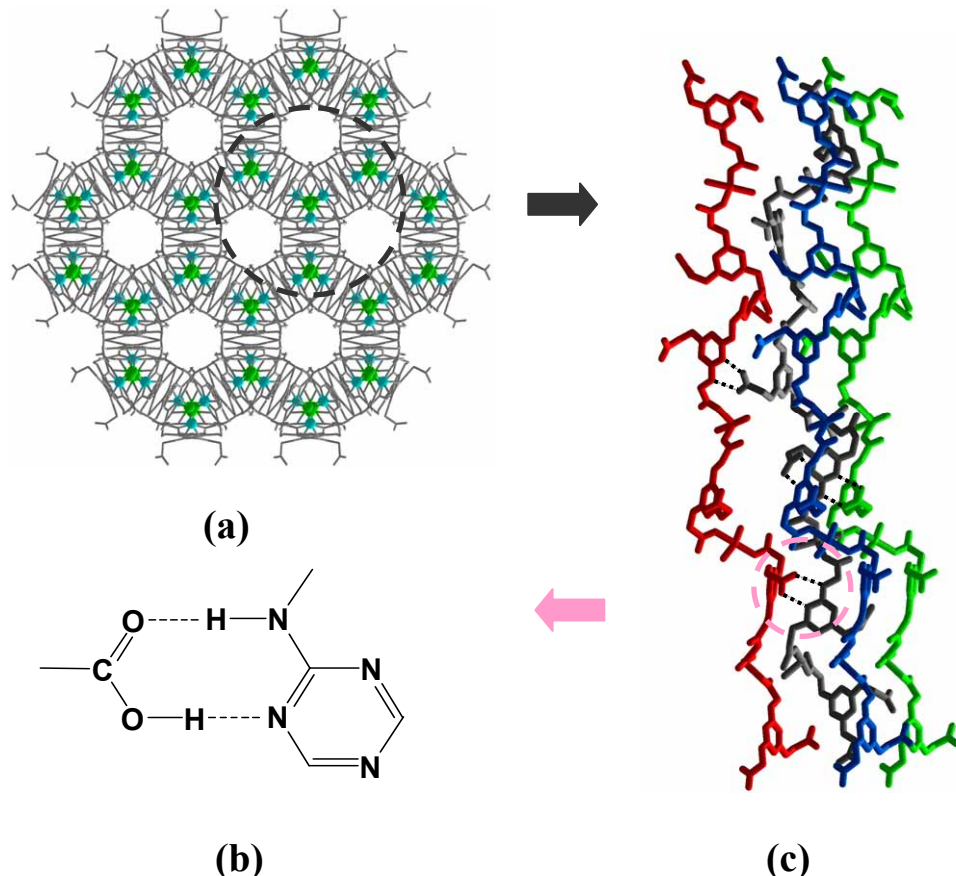
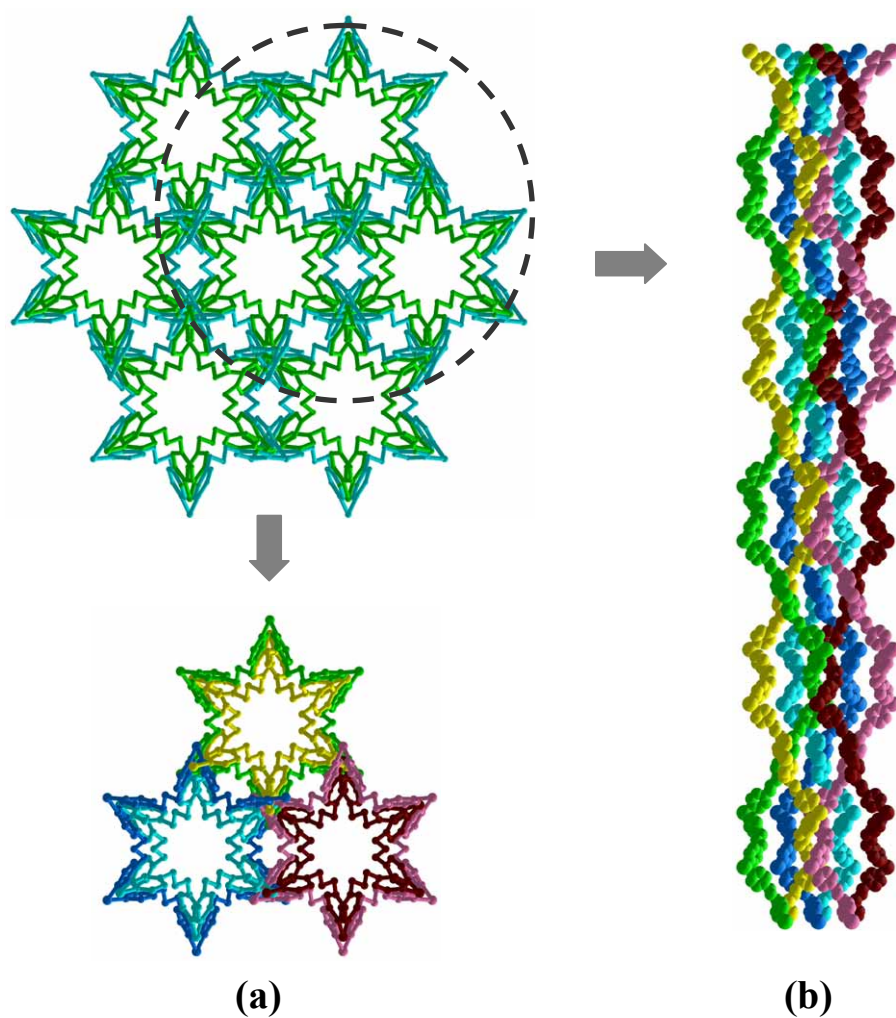


Figure S3. (a) The hexagonal arrangement of the metal-acid chains (**A**) in complex **1** viewed down the *c* axis. (b) $R_2^2(8)$ hydrogen bonding interactions. (c) Hydrogen bonding interactions between four adjacent **A** along the *b* axis.



Each metal-acid chain interacts with other three chains through $R_2^2(8)$ -type hydrogen bonds between the undeprotonated --COOH groups and the --NH-C=N-- groups. The $\text{N}\cdots\text{O}$ distance (2.666(5)-2.844(5) Å) and $\text{O--H}\cdots\text{N}$ (or $\text{N--H}\cdots\text{O}$) angles (151.7-160.2°) are both within ranges of those reported hydrogen bonds. As a result, all the chains are in hexagonal arrangements along the *c* axis, which may further stabilize the whole network. As far as we know, similar hydrogen bonds are common in organic system, but few examples of metal-organic frameworks have been documented up to now.

Figure S4. (a) View of the hexagonal arrangement of metal-base chains in complex 1 viewed down *c* axis. **B**, outer cycle; **C**, inner cycle. (b) View of three pairs of adjacent double helices along the *b* axis.



Bpp ligands adopt different *trans-trans* (*TT*) conformations with angles of pyridine rings of 79.0° and 69.6° to bridge Ni1 and Ni2 centers along the *c* axis, respectively, leading to metal-metal separation with Ni1...NiA and Ni2...Ni2B (symmetry codes: A, $1 + x - y, 2 - y, 2 - z$; B, $y, x, 5/3 - z$) of 13.850(4) Å and 12.874(4) Å, and thus two unequal coaxial left-handed helical chains (**B** and **C**). They possess the same long pitches of 62.471(3) Å with six metal centers and bpp ligands each. Interestingly, each pair of unequal coaxial double helices **B** and **C** intertwine with other six pairs of helical chains further, leading to aesthetic hexagonal arrangements along the *ab* plane. Though a limited examples of higher-order stranded helical complexes, including quadruple, quinduple, ninefold and tenfold, have been reported, such multiple-helical structures with two kinds of helices have not been documented.

Figure S5. Interweaving of the metal-acid chains with the metal-base chains viewed down *c* (top) and *b* (bottom) axis, respectively. (a) One metal-acid chain **A** assembled three pairs of double helices in **B₁C₃B₂C₁B₃C₂** sequence (**B_nC_n** represents one pair of double helical chains). (b) Each pair of **B** and **C** coil through six **A**.

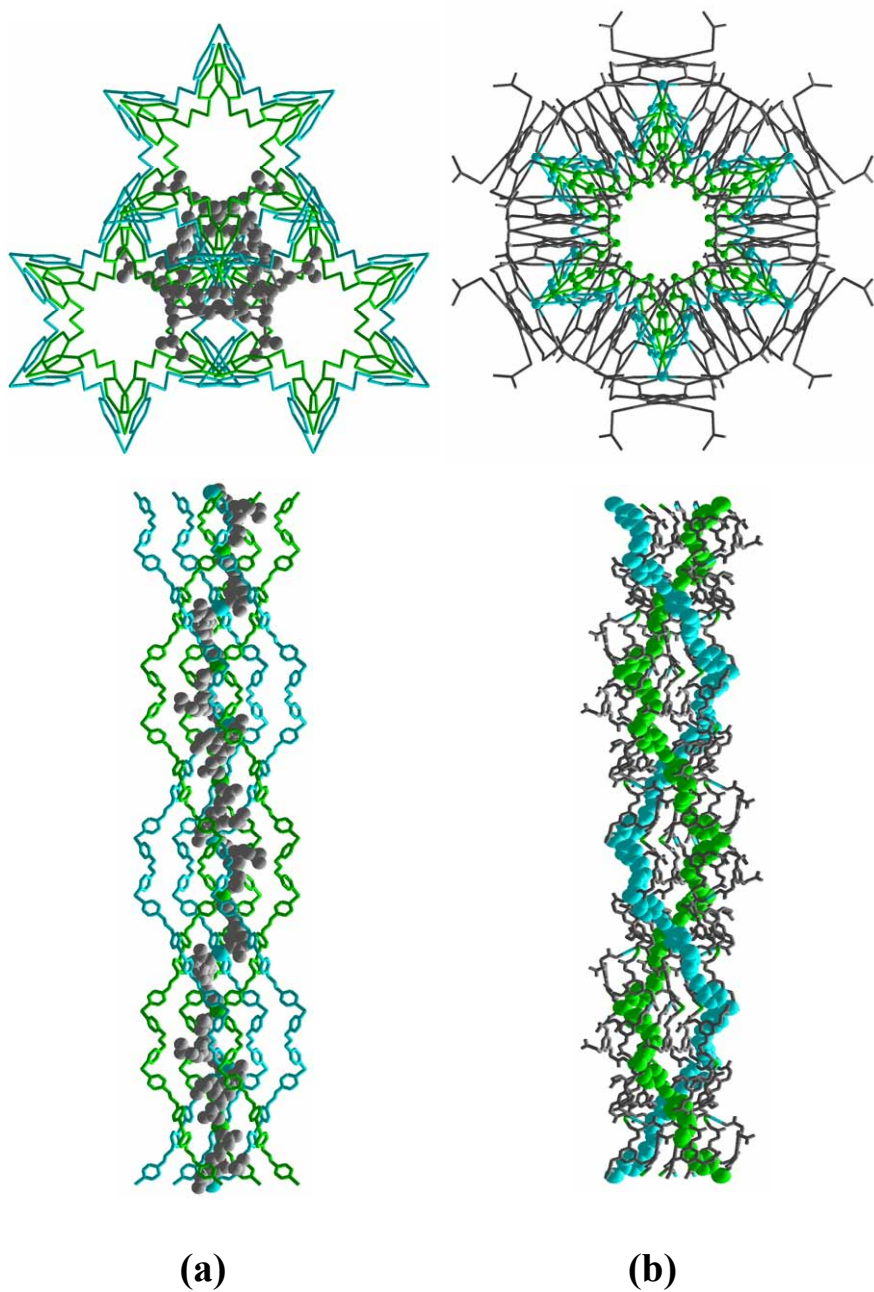


Figure S6. Scheme representation of the interweaving between **A** and **B**, **C**, showing one **A** with three pairs of double helices in $\mathbf{B}_1\mathbf{C}_3\mathbf{B}_2\mathbf{C}_1\mathbf{B}_3\mathbf{C}_2$ sequence ($\mathbf{B}_n\mathbf{C}_n$ represents one pair of double helical chains). The middle wide line with different colors represents **A**. The narrow lines represent chain **B** and **C**. \mathbf{B}_1 , red; \mathbf{B}_2 , sky blue; \mathbf{B}_3 , yellow; \mathbf{C}_1 , pink; \mathbf{C}_2 , mazarine; \mathbf{C}_3 , sap green.

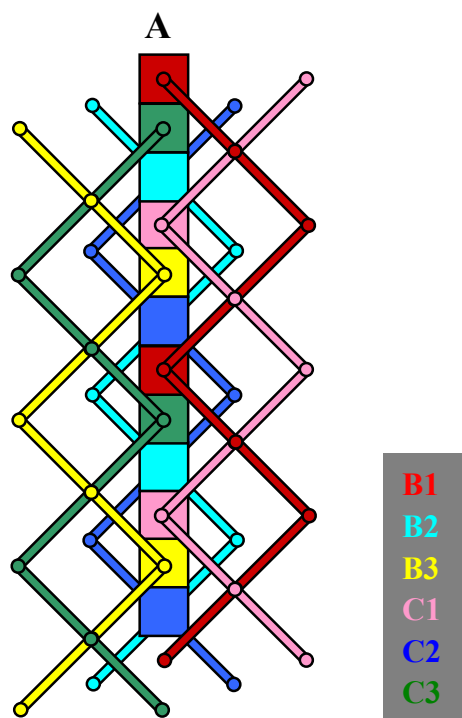
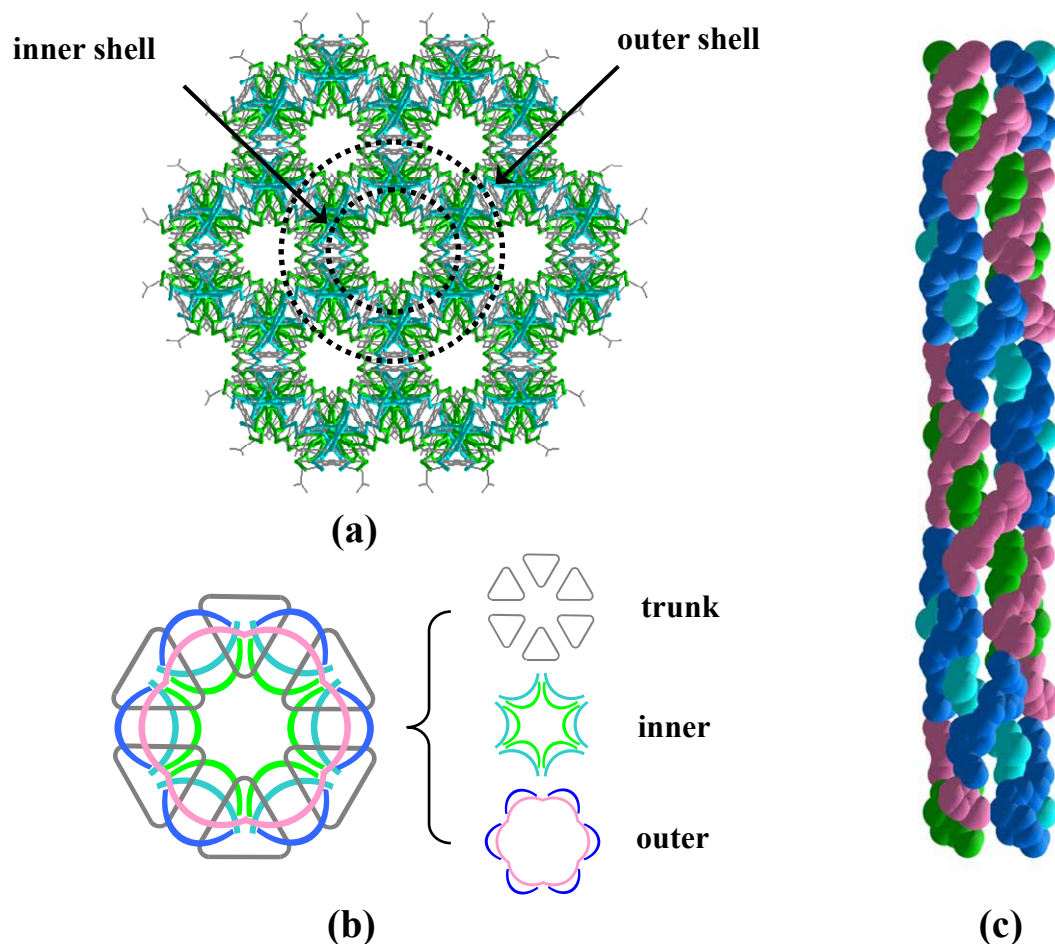


Figure S7. (a) View of the multi-walled tubular channels along the *c* axis. (b) Scheme representation of the three parts of the wall. (c) View of the channel along the *b* axis. The acid parts are omitted for clarity.



Inner shell: one pair of double helical metal-bpp chains (**B** and **C**)

Outershell: segments from six pairs of double helical chains of adjacent channels

Figure S8. (a) The repeat unit along the helical water chain in ball-and-stick representation. Hydrogen bonds are marked as blue broken lines. O, red; H, gray. (b) View of the helical water chain along the *c* axis. (c) Spacefilling of the helical water chains along the *b* axis. Gray sticks represent A, and only the hydrogen-bonded carboxylate groups are shown for clarity. Hydrogen bond, blue broken lines; Ni-O, green bonds.

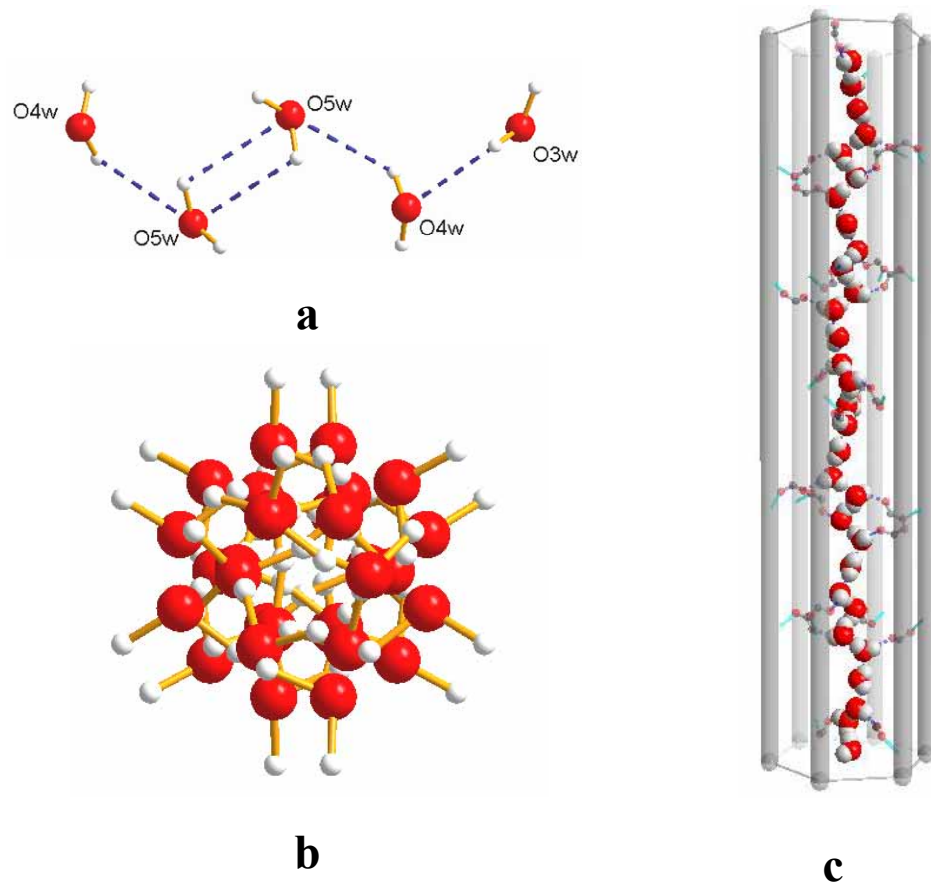
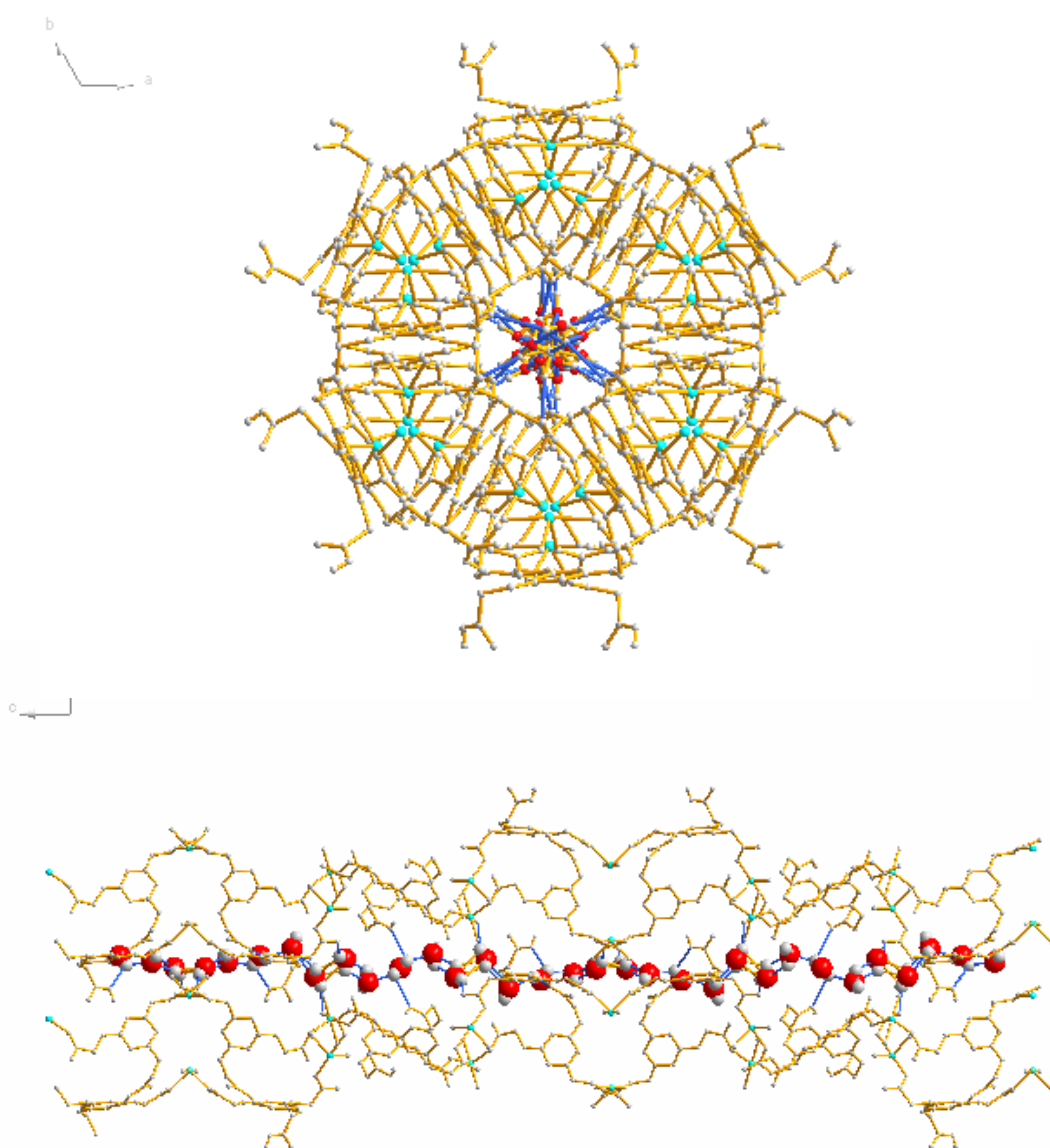


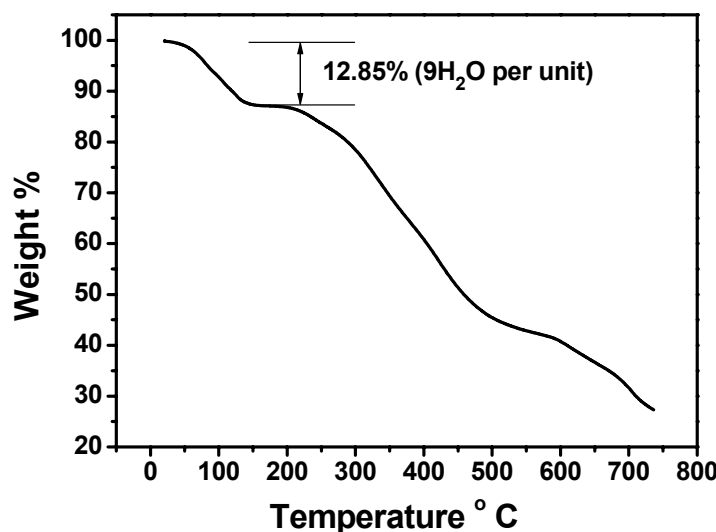
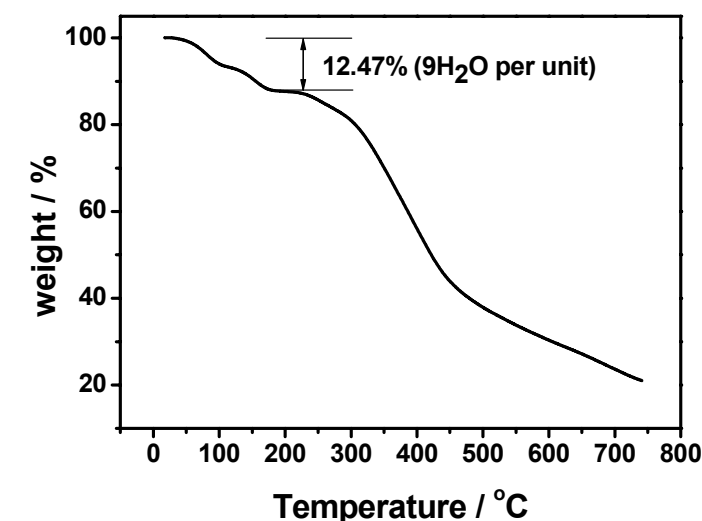
Figure S9. The hydrogen bonding interactions between the helical water chains and the host metal-frameworks viewed down the *c* (top) and *b* (bottom) axis, respectively. Broken blue lines represent hydrogen bonds.



All the lattice water molecules present in the asymmetric unit are inside the helical pore and involved in strong hydrogen bonds to produce a 1D helical polymer in the arrangement of $(-\text{O}3\text{w}-\text{O}4\text{w}-\text{O}5\text{w}-\text{O}5\text{w}-\text{O}4\text{w}-)_n$ with a 6_5 screw axis.

Furthermore, the helical water chains are anchored onto the host frameworks through hydrogen-bonding interactions between the uncoordinated carboxylate oxygen atoms ($O5w-H5wb...O2$ and $O4w-H4wb...O4$). And such weak interactions with right-handed helical host chains induce a right-handed helicity of the water chains with the long pitch of $62.471(3)$ Å.

Figure S10. DTA analysis of **1** and **2**.



Although of their isostructural nature, complexes **1** and **2** show slightly different properties due to the differences of the coordinated metal centers. TGA of complex **1** reveals a few stage processes. The first stage involves a 6.68% loss between 40 and

80°C, which is attributed to the loss of 5H₂O per unit (calculated 7.07%), and the second loss weight of 5.79% occurs between 80 and 150°C, suggesting the release of coordinated water molecules of 4H₂O (calculated 5.66%). No weight loss occurred until approximately 235°C, indicating the decomposition of the whole structure from then on. While for complex **2**, release of the solvent and coordinated water molecules is indistinguishable and all of them were lost in the range 40-140°C (9H₂O per unit, calculated 12.73%, found 12.85%) and the whole structure deposed at about 200°C.

Figure S11. XPRD pattern of the single crystal of complex **1** and **2** under different conditions. (a) Observed XPRD patterns of as-synthesized sample **1**. (b) Sample of **1** dried at 80°C under reduced pressure for 4 h; (c) Sample of **1** dried at 100°C under reduced pressure for 4 h; (d) H₂O immersed sample of **1** after drying. (e) Observed XPRD patterns of as-synthesized sample **2**. (f) Sample of **2** dried at 80°C under reduced pressure for 4 h; (g) H₂O immersed sample of **2** after drying.

After heated at 80°C under reduced pressure for 4h, the spectra of complex **1** were similar to the original ones, suggesting the crystalline is still maintained after removing the solvent molecules. Further heating the sample at 100°C for a while, all the peaks disappeared, indicating the crumbling of the whole structure. While for complex **2**, the collapse of the crystalline occurred at 80°C, indicating the slight difference between the coordinated metal atoms. After immersed in water for 12h, the dehydrated samples were transformed to the as-synthesized solids, suggesting the important roles of the guest molecules of water in the formation and stability of these compounds. The desolvated solids of these complexes may be potential reversible adsorbent materials for the water molecules.

